Earth Syst. Dynam. Discuss., 5, 1159–1196, 2014
www.earth-syst-dynam-discuss.net/5/1159/2014/
doi:10.5194/esdd-5-1159-2014

Earth System Dynamics Discussions
Open Access

A twelve-year high-resolution climatology of atmospheric water transport on the Tibetan Plateau

J. Curio[1], **F. Maussion**[1,2], **and D. Scherer**[1]

[1]Technische Universität Berlin, Chair of Climatology, Berlin, Germany
[2]University of Innsbruck, Institute of Meteorology and Geophysics, Innsbruck, Austria

Received: 7 September 2014 – Accepted: 19 September 2014 – Published: 2 October 2014

Correspondence to: J. Curio (julia.curio@tu-berlin.de)

Published by Copernicus Publications on behalf of the European Geosciences Union.

Abstract

The Tibetan Plateau (TP) plays a key role in the water cycle of High Asia and its downstream regions. The respective influence of the Indian and East Asian summer monsoon on TP precipitation and the regional water resources, together with the detection of moisture transport pathways and source regions are subject of recent research. In this study we present a twelve-year high-resolution climatology of the atmospheric water transport (AWT) on and towards the TP, using a new dataset, the High Asia Reanalysis (HAR), which better represents the complex topography of the TP and surrounding high mountain ranges than coarse resolution datasets. We focus on spatio-temporal patterns, vertical distribution and transport through the TP boundaries. The results show that the mid-latitude westerlies have a higher share in summertime AWT on the TP than assumed so far. Water vapour (WV) transport constitute the main part, whereby transports of water as cloud particles (CP) play also a role in winter in the Karakoram and western Himalayan regions. High mountain valleys in the Himalayas facilitate AWT from the south whereas the high mountain regions inhibit the AWT to a large extend and limit the influence of the Indian summer monsoon. No transport from the East Asian monsoon to the TP could be detected. Our results show that 40 % of the atmospheric moisture needed for precipitation comes from outside the TP, while the remaining 60 % are provided by local moisture recycling. How far precipitation variability can be explained by variable moisture supply has to be studied in future research by analysing the atmospheric dynamic and moisture recycling more in detail.

1 Introduction

The Tibetan Plateau (TP) is often referred to as the “world water tower” (Xu et al., 2008), being the origin of many big Asian rivers like the Indus, Ganges, Brahmaputra, Yellow River, Yangtze and Mekong. The TP is one of the most active centres in the word water cycle and constitutes an essential source of moisture for the downstream

ESDD
5, 1159–1196, 2014

regions in East Asia (Immerzeel et al., 2010). The transport of moisture to the TP is crucial for a sustainable water supply (Zhang et al., 2013). The moisture transport on and to the TP is influenced by mesoscale features (Sugimoto et al., 2008) but is also driven by large-scale atmospheric circulation: most notably the monsoon systems (Webster et al., 1998) and the mid-latitude westerlies (Schiemann et al., 2009). The unique topography of the TP, with its large extend and an average altitude of more than 4000 m makes it of particular interest because of its interaction with the large-scale circulation. The surrounding high mountain ranges, Himalaya, Karakoram, Pamir, Tien Shan and Kunlun Shan act as a barrier for the atmospheric moisture transport.

During the last decades the TP experienced climate changes towards warmer and wetter conditions (Yang et al., 2011, 2014), which have a direct impact on the hydrological cycle of the TP. Precipitable water (PW) shows increasing trends in the eastern and western TP and decreasing trends in the central TP (Lu et al., 2014). The poleward shift of the East Asian westerly jet in the period 1979–2011 and the intensification of the monsoon system are assumed to cause large areas of the TP to become wetter (Gao et al., 2014). Lake expansion in the central TP has intensified during last decades, due to global warming and its effects on the hydrological cycle of the TP (e.g. glacier retreat, permafrost degradation, Liu et al., 2010). The additional water vapour (WV), necessary for lake expansion, is assumed to come from outside the TP and therefore it is important to better understand the WV sources and transport processes (Yang et al., 2014).

Many studies about the atmospheric water transport (AWT) on and to the TP focus on the question how the Indian and East Asian summer monsoon systems imprint precipitation on the Tibetan Plateau, and how changes of the monsoonal circulation impact local and regional water resources (Gao et al., 2014; Immerzeel et al., 2013; Simmonds et al., 1999). In previous studies the influence of the westerlies and the monsoon system was examined on the basis of the precipitation timing and so supposed to be limited to winter (westerlies) or summer (Indian and East Asian summer monsoon) (e.g. Hren et al., 2009; Tian et al., 2007; Yang et al., 2014). The origin of the

ESDD
5, 1159–1196, 2014

atmospheric moisture on the TP plays a key role in recent research (e.g. Chen et al., 2012; Feng and Zhou, 2012). The general assumption is that the main WV source for summer precipitation on the TP is the Indian Summer Monsoon.

One method to identify the sources of moisture is to analyse the isotopic composition of precipitation, e.g. observed and modelled stable oxygen isotope ratio (δ^{18}O) and hydrogen isotope values (δD) (Araguás-Araguás and Froehlich, 1998; Tian et al., 2007; Yao et al., 2013), the isotopic composition of the water in rivers and smaller water streams (Hren et al., 2009), and of climate proxies like ice and sediment cores (Kang et al., 2007; Günther et al., 2011; An et al., 2012; Guenther et al., 2013; Joswiak et al., 2013). The latter ones can be used to analyse the moisture transport/conditions on the plateau and its source regions in the past. An et al. (2012) analysed a sediment core from the Lake Qinghai in the north east of the TP that reaches back 32 ka. They focused on the interplay of the westerlies and the Asian monsoon and showed that there is an anti-phase relationship with periods of dominant westerlies and periods with dominant Asian monsoon. Higher monsoon activity during the current warming period is found by studying variations in the monsoon intensity on the TP during the last 1000 years using data from sediment and ice cores (Günther et al., 2011). A shift in the isotope signals implies that the contribution of westerly moisture to the ice-core accumulation was relatively greater before the 1940s (Joswiak et al., 2013).

For the present day conditions various studies produce different results. Both the southern Indian Ocean (Indian summer monsoon) (Yao et al., 2013) and the Pacific Ocean (East Asian Monsoon) (Araguás-Araguás, 1998) are identified as the dominant moisture sources for summer precipitation on the TP. The analysis of stable isotopes of precipitation samples in west China show that the southern TP receives monsoon moisture in summer and westerly moisture in winter, while the moisture in western TP is delivered by the south-west monsoon (Tian et al., 2007). Hren et al. (2009), who sampled 191 stream waters across the TP and the Himalaya, found that the moisture entering the south-eastern TP through the Brahmaputra Channel originates in the Bay of Bengal. This monsoonal moisture is mixed with central Asian air masses the farther

ESDD
5, 1159–1196, 2014

west and north on the TP the sampling site is located. The role of local moisture recycling as an additionally moisture source is also emphasized in many studies (e.g. Joswiak et al., 2013; Kurita and Yamada, 2008; Trenberth, 1999). Araguás-Araguás (1998) found that it is dominant in winter and spring.

Another method to investigate the moisture transport on the TP are gridded atmospheric datasets e.g. global reanalysis data, regional atmospheric models or remote sensing data. Chen et al. (2012) used backward and forward trajectories to identify the sources and sinks of moisture for the TP in summer. Their results show that for periods longer than four days backwards, the main moisture source is the Arabian Sea, while for shorter periods the Bay of Bengal, the Arabian Sea, and the north-western part of the TP contribute moisture in the same order of magnitude. The results from the forward tracking underline the relevance of the TP moisture for the precipitation in East Asia. Feng and Zhou (2012) found that the main WV transport for summer precipitation takes place through the southern border of the TP and originates in the Bay of Bengal and the Indian Ocean. They also point out that the southern branch of the midlatitude westerlies transports moisture to the TP too, but its share is distinctly lower. Lu et al. (2014) analysed the atmospheric conditions and pathways of moisture to the TP for a wet and a dry monsoon season and showed that differences in the atmospheric circulation have a direct impact on the moisture transport and on the PW over the TP. Meridionally orientated high mountain valleys in the Himalayas can channel water vapour and precipitation to the TP (Bookhagen and Burbank, 2010).

Previous studies relied on global reanalysis datasets to quantify the transport to the TP. Recently, a new high-resolution dataset, the High Asia Reanalysis (HAR; Maussion et al., 2014), was made available. With a high spatial (30 and 10 km) and temporal (3 and 1 h) resolution the dataset allows us to analyse the AWT above the Tibetan Plateau differentiated in space and time. By using this new dataset with a distinct higher horizontal resolution than the global datasets the question arises if the more realistic representation of the topography of the TP and the surrounding high mountain ranges leads to an improvement in atmospheric moisture re-presentation.

ESDD
5, 1159–1196, 2014

The objectives of the current study are threefold:

i. Describe the characteristics of the AWT on and to the TP as resolved by the HAR dataset during the last decade, with focus on spatial patterns, seasonal evolution and vertical distribution,

ii. examine the barrier effect of the topography on the AWT and detect the major transport channels to the plateau,

iii. and quantify the importance of increasing model spatial resolution on these transport channels.

Here we present a twelve-year climatology of atmospheric water transport (AWT) over the TP and adjacent mountain ranges based on the HAR. We focus on the period 2001–2012 (referred to the "last decade" for convenience). First, we will look at the mean annual cycle of the AWT (water vapour and cloud particles) to detect the mean patterns and transport channels. The vertical distribution of the transport is then analysed using selected model levels We also compute vertical cross sections along the border of the TP to quantify the atmospheric water input and verify the importance of the detected transport channels. In a final step we will calculate an estimation of the budget of the AWT and its share on the precipitation falling on the TP.

2 Data and methods

2.1 The HAR dataset

We use meteorological fields provided by the High Asia Reanalysis (HAR). The HAR is generated by using the advanced research version of the Weather and Research Forecasting model (WRF-ARW, Skamarock and Klemp, 2008) version 3.3.1, used to downscale the Operational Model Global Tropospheric Analyses (Final Analyses, FNL; dataset ds083.2), which are available every six hours and have a spatial resolution of

ESDD
5, 1159–1196, 2014

one degree. It provides products at a spatial resolution of 30 km and temporal resolution of three hours for the first domain, covering most parts of central Asia (HAR30). A second nested domain (HAR10) covers High Asia and the TP with a spatial resolution of 10 km and temporal resolution of one hour (Fig. 1). The dataset is available online at http://www.klima.tu-berlin.de/HAR and described in detail by Maussion et al. (2011, 2014). The HAR provides meteorological fields at the surface and on 28 terrain-following vertical sigma levels. The dataset covers a period of more than twelve years from October 2000 to December 2012 and is updated continuously. HAR products are available for different time aggregation levels: hourly (original temporal model resolution), daily, monthly and yearly.

The HAR precipitation data were compared to rain gauge observation and precipitation estimates from the Tropical Rainfall measuring Mission (TRMM) by Maussion et al. (2011, 2014).

2.2 Moisture transport

Atmospheric water transport happens through WV transport of cloud particles (CP). In this study we are interested in CP transport but do not further distinguish between liquid (water droplets) and solid (ice) cloud particles which are both resolved by the model microphysics. WV and CP fluxes are calculated for each of the 28 original sigma levels, which are terrain following, based on the original temporal model resolution of 1 h (HAR10) and 3 h (HAR30) using the formula:

$$Q = \boldsymbol{v}_{\mathrm{h}} \rho q \Delta z \tag{1}$$

where Q is the water vapour flux ($\mathrm{kg\,m^{-1}\,s^{-1}}$) or cloud particles flux, $\boldsymbol{v}_{\mathrm{h}}$ denotes the horizontal wind vector ($\mathrm{m\,s^{-1}}$), ρ is the dry air density ($\mathrm{kg\,m^{-3}}$) and q is the specific humidity ($\mathrm{kg\,kg^{-1}}$). Δz is the thickness of each sigma level (m), this value is not constant but increases with increasing height above ground. Since the WRF model just provides mixing ratios (r) for the three atmospheric water components (water vapour, liquid water and ice), we first calculated the specific humidity for each component using the relation:

ESDD
5, 1159–1196, 2014

$$q = \frac{r}{(1+r)} \tag{2}$$

Additionally we integrated the fluxes over the whole atmospheric column to gain the vertically integrated atmospheric water transport fluxes. The vertical integration is performed along the metric z-coordinate along the model sigma levels from surface to top using the rectangle method.

$$Q = \int_{z=z_{\mathrm{top}}}^{z=z_{\mathrm{sfc}}} \boldsymbol{v}_{\mathrm{h}} \rho q \, \Delta z \tag{3}$$

We calculated these fluxes for the original model levels and did not interpolate them to pressure levels to avoid information loss due to the interpolation. For the analyses, 10 and 5 grid points from the HAR30 and HAR10 domain boundaries, respectively, are removed to avoid lateral boundary effects.

To analyse the AWT towards the TP, we compute vertical cross sections along transects following the border of the TP. To be able to calculate a moisture budget, we framed/surrounded a region which we call from now on "the inner TP", with 14 transects trying to follow the highest elevations in the mountain ranges and to cut the high mountain valleys which we assume to be pathways for atmospheric moisture. A map with the transects is shown in Fig. 1. The *u*- and *v*-components of the AWT are then rotated to the transect coordinate system to compute the normal fluxes towards the cross section.

2.3 ERA-Interim

To examine if our dataset is able to reproduce the general characteristics of the WV flux, we compare the WV fluxes derived from HAR30 with ERA-Interim Reanalysis data (Dee et al., 2011). The ERA-Interim WV fluxes are available online as an integral over

ESDD
5, 1159–1196, 2014

the atmospheric column for the eastward (u) and northward (v) components as monthly means. ERA-Interim has a horizontal resolution of 0.75°. To calculate the differences between the HAR30 and ERA-Interim WV fluxes, we transformed HAR30 data to the ERA-Interim grid by averaging the HAR30 grid points below each ERA-Interim grid point. The u- and v-components of the HAR fluxes were rotated to earth coordinates first.

3 Results

3.1 Comparison of HAR30 with ERA-Interim water vapour fluxes

The general patterns and the magnitude of the WV transport amounts of HAR30 and ERA-Interim are in agreement (Fig. 2). Figure 2c shows the differences between HAR30 and ERA-Interim for July when the largest differences were found. The main differences between the two datasets are visible south of the eastern and central Tibetan Plateau along the southern slopes of the Himalayas. The WV transport through the Brahmaputra Channel towards the Tibetan Plateau is higher for ERA-Interim than for HAR30. This is probably due to differences in the representation of the orography, caused by different horizontal resolutions. HAR30 produces more transport westward along the Himalayas (upstream the Ganges river), which is caused by more WV blockage. When the WV flux hits the Himalayas from the south it is mostly redirected to the west and follows the southern slopes of the Himalayas. In winter the differences are in general less pronounced (not shown).

3.2 Climatology of the atmospheric water transport (AWT)

Figure 3 displays the December–February (DJF) (left) and June–August (JJA) (right) decadal average of the vertically integrated atmospheric water transport (AWT) derived from HAR30. In winter (DJF) the AWT from west to east is dominant over the TP and most parts of High Asia. In the tropical ocean region we have transport from

ESDD
5, 1159–1196, 2014

east to west with the trade winds. The TP and the regions north of the plateau show small transport amounts, below 40 kg m^{-1} s^{-1}. For comparison, the AWT reaches up to 450 kg m^{-1} s^{-1} over the South Chinese Sea off the coast of Vietnam. In summer (JJA) the pattern in the southern part of the domain is completely different from winter due to the circulation change related to the Indian Summer Monsoon (ISM). The largest amount of atmospheric water is now transported from west to east over the Arabian Sea and the Bay of Bengal. Over the Bay of Bengal the flow gets a larger southerly component, and atmospheric water is directly transported to the southern slopes of the Himalayas. Over the TP the transport amount is still low in comparison.

3.2.1 Annual cycle of HAR10 water vapour (WV) transport

The annual cycle of vertically integrated WV transport (monthly decadal average) is provided in Fig. 4, and the WV transport spatially averaged for the inner TP is shown in Fig. 5. In winter the westerlies are dominant in the whole domain, and therefore the available WV is transported eastward. The highest amounts of WV transport (50–200 kg m^{-1} s^{-1}) occur south of the Himalayas. On the TP the WV transport amount is distinctly lower (10–50 kg m^{-1} s^{-1}). The WV transport towards the TP can just takes place through some high mountain valleys at the south-western border of the TP (Western Himalayas, Karakoram, Pamir) and in the south-east of the TP where the Brahmaputra Channel is located. Additionally, the atmosphere over the TP is cold in winter and cannot hold large amounts of WV. The transport of WV on the TP further to the east is facilitated by lower elevated west-east orientated regions like the Yarlong Zhangpo (Brahmaputra) river course in the south. Therefore, the highest transport amounts are visible in the south-eastern and central southern TP.

From May to July the amount of transported WV in in these regions increases and the region with higher transport extends to the central TP. This intensification of the transport is also visible in Fig. 5a and takes place before the actual monsoon season. Already in May the WV flux south-east of the Himalayas gets a more southerly component and the WV is no longer transported along the southern slopes but hits the

ESDD
5, 1159–1196, 2014

mountain ranges from the south. This results in an increase of the AWT amount north of the Himalayas. Due to the further evolution of the Indian Summer Monsoon, the transport intensifies over summer. However, large amounts of AWT from the Bay of Bengal northward to the Himalayas are blocked by the orographic barrier and redirected westward. This leads to high amounts of WV transport along the southern slopes of the Himalayas following the Ganges river course to the west. WV transport to the TP is possible where meridionally orientated valleys along this course exist.

The WV transport through the south-western border of the TP also increases over summer. This WV is not transported towards the TP by the monsoonal flow, but is provided by the southern branch of the mid-latitude westerlies. This is clearly visible in the transport patterns of the HAR30 domain (Fig. 3). Another hint for the contribution of the westerlies to the WV transport on the TP is the dominant transport direction in the southern TP from west to east. This eastward transport starts further west than the monsoonal flow reaches along the southern slopes. So the WV from the Bay of Bengal cannot be the major source of the moisture transported in the westernmost regions of the TP.

In summer the WV transport over the Qaidam Basin from north-west southward is nearly as high as in the monsoonal affected south-east of the TP. Figure 6, representing the decadal monthly average of HAR10 precipitation, shows that we have a precipitation minimum in this region in summer, although large amounts of WV are transported to this region. Convection might be hindered by subsidence or high wind speeds (wind shear effect).

In September we have the highest WV transport amounts over the TP. This intensification of the water vapour transport occurs because the precipitation in September (Fig. 6) is low compared to the summer months. The surface is wet due to the high precipitation rates in July and August and the temperatures are still relatively high, which leads to high evaporation from the land surface. The evaporated moisture can be transported away from the source region and will not be rained out over the TP. In October there is only transport to the TP in the eastern and central parts of the Himalayas,

ESDD
5, 1159–1196, 2014

because the monsoon circulation weakens and the fluxes does not reach as far as before westward into the Ganges valley. The flux from the westerlies reaches far more to the east along the southern slopes of the Himalayas (TP). In November this pattern becomes more intense and there is no westward flux south of the Himalayas visible, the monsoon circulation is collapsed and the wintertime situation is established.

3.2.2 HAR10 cloud particles (CP) transport

The median value of HAR10 WV transport for the inner TP is between 20 and 40 $\mathrm{kg\,m^{-1}\,s^{-1}}$ over the whole year, while it is between 0.2 and 0.6 $\mathrm{kg\,m^{-1}\,s^{-1}}$ for the CP transport (Fig. 5). Differences in the annual cycle of the two components are clearly visible, the WV transport has its peak in summer, the CP transport in winter. To examine the relevance of CP transport for the AWT, we looked at the transport patterns and amounts and calculated the contribution of the CP flux to the AWT as a monthly decadal average in January and in July (Fig. 7). It shows that in winter in the Karakoram/Pamir/Western Himalayas region the CP flux can account for up to 25 % of the entire AWT. This pattern matches with the wintertime precipitation pattern in this region (Fig. 6). From April on (not shown), we have relatively high transport amounts (up to 2–3 $\mathrm{kg\,m^{-1}\,s^{-1}}$) in the south-east of the domain, but in summer the CP transport amount decreases in this two regions to very small values. Just over the central eastern parts of the Plateau the amount increases and is around 8 % of the AWT. The percentage of CP on the AWT is higher at higher elevations where the WV transport is lower because of lower temperatures. The relatively high percentage values over the Tarim Basin are related to the low AWT in general in this region.

3.3 Vertical structure of the atmospheric water transport

We display the decadal average of HAR10 AWT for selected vertical levels in Fig. 8. We selected the levels 1 (~ 25 m above ground in Tibet), 5 (~ 450 m above ground in Tibet), 8 (~ 1200 m above ground in Tibet), 10 (~ 2200 m above ground in Tibet), 12

ESDD
5, 1159–1196, 2014

(∼ 3200 m above ground in Tibet) and 15 (∼ 5500 m above ground in Tibet), because these levels show the most interesting features of the WV transport. The WV transport near the ground (level 1) is generally low on the TP and just a little bit higher south of the Himalayas, probably because of the lower surface wind speeds and of the stronger mixing in the boundary layer. The transport amount increases strongly up to level 12, where the largest transport occurs, due to higher wind speeds, higher moisture availability or both. Above this level the WV transport starts to decrease and above level 17 (not shown) the transport amount is close to zero.

The general atmospheric circulation at different levels is visible in the transport patterns, but we have to consider that the AWT is a complex mixture of wind and moisture availability. At the lower levels (1 and 5) we see the cyclonic circulation around the Tibetan heat low, with its centre in the central TP. At level 8 this structure is shifted to the central northern TP. Level 12 and 15 (and levels in between) show an anticyclonic circulation around a centre at the southern TP, directly north of the Himalayas. In level 15 and 16 a second anticyclonic circulation is visible in the south east of the domain, directly south of the Himalayas. Above these levels the anticyclonic circulation slowly weakens and a division in a northern part with transport from west to east, where the westerlies are dominant, and a southern part with transport from east to west is visible. Level 10, which lays between these circulation features, could be called the equilibrium level.

At level 5 monsoonal air and moisture is transported relatively far to the western (north-western) parts of the TP. Air from the south which originates in the tropical oceans (Indian summer monsoon) is included in the cyclonic circulation over the TP, but the WV does not seem to originate from the East Asian monsoon. In the higher levels (10–15), this cyclonic circulation is replaced by the westerlies and therefore extratropical air masses are transported to this region. Therefore we have air masses and consequently moisture from different sources at one place. This result should be considered for the analysis of stable oxygen isotopes in precipitation samples, lake water, sediment and ice cores. Precipitation originating in the boundary layer will result in

ESDD
5, 1159–1196, 2014

a monsoonal signal in the isotopes while precipitation originating from deep convection could have an isotope signature that will be dedicated to the westerlies.

In the dry Tarim Basin north of the TP we can see an anticyclonic circulation above the boundary layer at level 10 and transport of WV from north-east to south-west following the northern boundary of the TP. Therefore, the air at this level tends to descent and just boundary layer clouds are possible below this level, which can provide just small amounts of precipitation. Above this level the transport of WV is admittedly higher and to the opposing direction, but does not result in precipitation. Deep convection is inhibited by the subsidence tendency at the lower level.

In the south-western parts of the domain, in the border region between India and Pakistan, we can see the same feature but there it leads to higher differences in the precipitation patterns and affects a region with a higher population density. We see an anticyclonic circulation of the WV transport in the levels 10 and 12 (and in between). The transported amount is nearly as high as the WV transport associated with the ISM along the southern slopes of the Himalayas. But if we look at the precipitation patterns we see that there is a precipitation minimum in this region (Fig. 6). The development of deep convection is suppressed by the subsidence. In the lower levels we have a cyclonic movement of the air masses which is visible in the transport patterns (Fig. 8) and in the 10 m wind field (Fig. 6). In the surrounding region where we do not see this anticyclonic movement in the levels above the boundary layer, the large amounts of transported WV result in high amounts of precipitation. This result can provide an indication of the processes, which lead to the risk of droughts in Pakistan.

3.4 Transport towards the Tibetan Plateau through its borders

We calculated the HAR10 WV input towards the TP through its borders (Figs. 9–12 and Table 1). For the southern boundary cross sections (CS 2–6) the highest transport amounts occur in summer (Fig. 9), in the lower layers and decreases with increasing height. The largest fluxes occur in the regions where the elevation is lower compared to the direct surroundings, the large meridionally orientated valleys (eastern Himalayas, in

ESDD
5, 1159–1196, 2014

the region of the Brahmaputra channel). There, the areas of lower elevation are wider, and the AWT from the Indian Ocean hits the mountain ranges directly from the south.

The AWT from the TP to the south is negligible in summer (Fig. 9). It occurs mainly at CS 2 and a bit at CS 3. Maybe this is a kind of recirculation of northward transport. It takes place in the lower levels above a layer with high northward transport amounts. In winter (Fig. 10) the AWT is lower but the input of atmospheric moisture is still dominant.

The AWT through the western boundary (CS 1) (Figs. 9 and 10 and Table 1) is higher in winter than in summer as it is for CS 2 in the westernmost region of the Himalayas. These regions are dominated by input atmospheric water originating in extra-tropical air masses, transported to this region by the westerlies. In sum the AWT at CS 2 is still almost as high as the AWT at CS 6. CS 6 contains the Brahmaputra Channel, which is often referred to as the main input channel for atmospheric moisture.

Table 1 shows the monthly decadal average of the AWT input to the TP through the individual cross sections converted to a theoretical equivalent precipitation amount on the inner TP. We picked the CS 1 and CS 6 for a closer comparison because CS 6 includes the Brahmaputra Channel and CS 1 is the western boundary, and they are of the same length. From November to April the transport through the western boundary (CS 1) is distinct higher than that through CS 6. From May to October CS 6 shows higher transport amounts, but the differences are lower than for the winter time. In July the ratio between CS 1 and CS 6 is 90.47 %, which means that the input through the western boundary is around 90 % of the transport through the Brahmaputra Channel region. This is the month where the differences are smallest. We can see that CS 2–3 for almost every month exhibits the largest input amounts. The AWT through this cross section is controlled not only by the ISM but also by the southern branch of the mid-latitude westerlies.

The cross section for the eastern boundary (CS 7) shows that the TP is a source of atmospheric water to the downstream regions east of the TP for all months (Table 1 and Figs. 11 and 12). In January we have only eastward transport through the eastern boundary (Fig. 11) In the other months (not shown except of July, Fig. 12) we have

ESDD
5, 1159–1196, 2014

additionally transport towards the TP in the lower layers near the surface. The transport towards the TP through eastern cross section has its peak in July (Fig. 12) in the northern parts of the boundary where the elevation is distinct lower than in the southern parts. Above this region there is still eastward AWT away from the TP. However, if we look at the total of the AWT amount through the eastern boundary, we see that the transport from the Plateau towards the east is dominant also in summer, although we see this low level high transport amounts towards the TP.

The transport through the northern boundary (CS 14–8) towards the TP (input) is lower than from west and south in January and July (Figs. 11 and 12, Table 1). There we have a strong gradient in altitude and fewer passages, through which the atmospheric water could enter the TP, than in the Himalayas, although the circulation is directed to the boundary of the TP especially in summer. For the westernmost northern cross sections (14–12) the transport from the TP to the north is dominant because we have north-eastward transport on the western TP, this is another reason for the lower transport amounts towards the TP. The AWT with the northern branch of the westerlies north of the TP is blocked by the high elevated TP and then follows its northern border to the east, where the elevation is lower in some regions (CS 9–11), e.g. at the border to the Qaidam Basin (CS 9). There, the input of atmospheric water to the TP is dominant for all months and the maximum input takes place in spring. The AWT from the north to the Qaidam Basin is also visible in Fig. 4 for all months. This transport takes place in the lower layers of the atmosphere. The transport from the Plateau northwards has its peak at the easternmost northern CS (CS 8) in July, August and September, when the TP can provide large amounts of atmospheric water, like shown in Sect. 3.2.1 in Fig. 4.

3.5 Budget

Since we analysed the AWT transport on and to the TP and quantified the in- and output, the question arises, which amount of precipitation falling on the inner TP results

ESDD
5, 1159–1196, 2014

from external moisture supply and which amount is provided by the TP itself by local sources and moisture recycling?

Table 1 displays the monthly decadal average of the AWT through the HAR10 individual cross sections and the sum for all cross sections, the HAR10 precipitation falling on the inner TP and the ratios between them. To make the comparison with the precipitation easier we converted the net atmospheric water input to a theoretical precipitation equivalent (mm month^{-1}). We obtain an annual mean AWT input of 220.5 mm yr^{-1} for HAR10. For the mean annual precipitation falling on the inner TP, a value of 544.8 mm yr^{-1} results. The ratio of net input of atmospheric water to the precipitation falling on the inner TP reveals that on average the AWT through the borders accounts for 40 % of the precipitation during the year. According to that the remaining 60 % of atmospheric water needed for precipitation must be provided by the TP itself. This moisture supply probably takes place via moisture recycling from local sources, e.g. evaporation from numerous and large lakes, soil moisture, the active layer of permafrost, snow melt and glacier run-off. The ratio is highest in winter when the TP cannot provide moisture for precipitation by itself, followed by summer, where the largest net input occurs. In October and November the ratio is negative, which means that the TP provides more moisture than it receives from external sources. On a monthly basis there is certainly a time lag between the moisture entrance and the precipitation, what makes the analysis of the monthly ratios difficult.

4 Discussion

The main WV output from the TP takes place through the eastern border, as found by Feng and Zhou (2012) too. The TP is a source of moisture for the downstream regions in the east throughout the year like the Yangtze river valley in China and so we can confirm the finding from Bin et al. (2013), who called the TP a transfer platform of moisture for the downstream regions in East Asia. Our results also match with the findings of

ESDD
5, 1159–1196, 2014

Mölg et al. (2013), who found out that the westerlies play a role for precipitation and glacier mass balance also in summer.

In our study we could not find any contribution of the East Asian Summer Monsoon to the WV transport towards the TP. The WV transported from east to the TP in summer (CS7, Fig. 12) is not transported to this region by the East Asian Monsoon flow but by the eastern branch of the Indian Summer Monsoon flow. This is clear if we look at the transport patterns for HAR30 (Fig. 3). It is interesting that the HAR WV flux has a stronger westward component east of the TP than ERA-Interim (Fig. 2c) and still does not show any transport from east to west.

Prior studies focused on the WV transport and did not considered the CP flux. The assumption so far was that the CP transport is so small compared to the WV flux, that it does not has a significant influence on the atmospheric moisture transport. Our results show that the contribution of the CP flux to the entire AWT is not negligible in winter in the Pamir and Karakoram (the western and south-western border of the TP), where it contributes up to 25 % of the entire AWT. The fact that the CP transport plays a role in the Karakoram and western Himalayas, the regions which are controlled mainly by the westerlies, lets conclude that in this region moisture advection presumably plays a strong role. The horizontal motion is dominant in advective processes towards convection where the vertical motion is dominant. This leads to the fact that clouds developed in advective processes, for example frontal processes, can be transported further away from their origin than convective clouds.

The moisture supply from external sources provides around 40 % of the atmospheric water needed to produce the mean annual precipitation on the inner TP while the remaining part originates from the TP itself by local moisture recycling. This moisture is provided by the evaporation from numerous and large lakes, soil moisture, the active layer of permafrost, snow melt and glacier run-off. The question arises what will happen with the atmospheric water, which is transported to the TP? Does it remain on the TP or does it run off? Could this moisture input be an explanation for the observed lake level rises?

ESDD
5, 1159–1196, 2014

The comparison of the net atmospheric water input to the TP through the cross sections, the precipitation falling on the inner TP and the ratio between them for HAR10 (Table 1) and HAR30 (Table 2) shows that the different horizontal resolutions result in differences between the two datasets. On an annual basis the different horizontal resolutions result in an AWT input difference of 60 mm yr^{-1} and a precipitation difference on the inner TP of 22 mm yr^{-1}. The HAR30 net atmospheric water input accounts for 28 % of the precipitation, so this results in a difference of 12 % to HAR10 dataset. Nevertheless, HAR30 has almost for every cross section and month higher transport amounts for both in- and output. Due to the fact that also the output values are higher the annual net input for HAR30 is lower than for HAR10. A possible explanation for lower transport amounts for individual cross sections in HAR10 could be that the higher horizontal resolution is overridden by higher orographic barriers due to better representation of the topography. Shi et al. (2008) showed that a higher horizontal resolution and more realistic representation of the topography is important for the development of disturbances leading to precipitation events in the downstream regions of the TP like the Yangtze River valley. Our study shows that for a quantification of the AWT and the spatio-temporal detection of its major pathways and sources it is important to consider the complex topography of High Asia spatially high resolved.

5 Conclusions

The TP experiences high precipitation variability leading to dry spells and droughts, as well as to severe snow- and rainfall events and subsequent floods. However, there are strong differences between regions and seasons, which are not yet well understood for present-day climate conditions, making statements for past and future climates highly speculative. Therefore, in a further study we will analyse if there are significant differences in the AWT patterns in wet and dry years, to find out, whether the extremes are influenced by changes in atmospheric circulations or just in a change of the transported amount of atmospheric water. This results then could be compared with the results of

ESDD
5, 1159–1196, 2014

Lu et al. (2014), who analysed the differences in the atmospheric circulation for wet and dry monsoon seasons of nearly the same period (2000–2010) using coarser resolution datasets. Interesting regional features, like the large amount of atmospheric water over the dry Qaidam Basin which does not result in precipitation, need to be studied in detail by analysing the reasons for precipitation suppression. Dust particles originating in the arid regions could even play a role in precipitation suppression (Han et al., 2009).

Our first water budget estimate reveals that local moisture recycling is an important factor and provides more moisture than the input from external sources (on average 60 % vs. 40 %). The moisture recycling has to be studied more in detail in the future to gain a better understanding of the water cycle on the TP. It would be interesting to analyse how and if the atmospheric water stored in snow in winter contributes to the atmospheric water transports and precipitation of the following warm season. Due to this storage term the westerlies maybe could play an even greater role in the hydrological cycle of some regions of the TP in summer. Additionally the other components of the water balance, e.g. evaporation and run off should be considered in further studies.

Acknowledgements. This work was supported by the German Federal Ministry of Education and Research (BMBF) Programme "Central Asia – Monsoon Dynamics and Geo-Ecosystems" (CAME) within the WET project ("Variability and Trends in Water Balance Components of Benchmark Drainage Basins on the Tibetan Plateau") under the code 03G0804A and by the German Research Foundation (DFG) Priority Programme 1372, "Tibetan Plateau: Formation – Climate – Ecosystems" within the DynRG-TiP ("Dynamic Response of Glaciers on the Tibetan Plateau to Climate Change") project under the codes SCHE 750/4-1, SCHE750/4-2, SCHE 750/4-3. F. Maussion acknowledges support by the Austrian Science Fund (FWF project P22106-N21).

ESDD
5, 1159–1196, 2014

References

An, Z., Colman, S. M., Zhou, W., Li, X., Brown, E. T., Jull, A. J. T., Cai, Y., Huang, Y., Lu, X., Chang, H., Song, Y., Sun, Y., Xu, H., Liu, W., Jin, Z., Liu, X., Cheng, P., Liu, Y., Ai, L., Li, X., Liu, X., Yan, L., Shi, Z., Wang, X., Wu, F., Qiang, X., Dong, J., Lu, F., and Xu, X.: Interplay between the Westerlies and Asian monsoon recorded in lake Qinghai sediments since 32 ka, Sci. Rep., 2, 619, doi:10.1038/srep00619, 2012.

Araguás-Araguás, L., Froehlich, K., and Rozanski, K.: Stable isotope composition of precipitation over southeast Asia, J. Geophys. Res., 103, 28721–28742, doi:10.1029/98JD02582, 1998.

Bin, C., Xiang-De, X., and Tianliang, Z.: Main moisture sources affecting lower Yangtze river basin in boreal summers during 2004–2009, Int. J. Climatol., 33, 1035–1046, doi:10.1002/joc.3495, 2013.

Bookhagen, B. and Burbank, D. W.: Toward a complete Himalayan hydrological budget: spatiotemporal distribution of snowmelt and rainfall and their impact on river discharge, J. Geophys. Res., 115, F03019, doi:10.1029/2009JF001426, 2010.

Chen, B., Xu, X.-D., Yang, S., and Zhang, W.: On the origin and destination of atmospheric moisture and air mass over the Tibetan Plateau, Theor. Appl. Climatol., 110, 423–435, doi:10.1007/s00704-012-0641-y, 2012.

Dee, D. P., Uppala, S. M., Simmons, A. J., Berrisford, P., Poli, P., Kobayashi, S., Andrae, U., Balmaseda, M. A., Balsamo, G., Bauer, P., Bechtold, P., Beljaars, A. C. M., van de Berg, L., Bidlot, J., Bormann, N., Delsol, C., Dragani, R., Fuentes, M., Geer, A. J., Haimberger, L., Healy, S. B., Hersbach, H., Hólm, E. V., Isaksen, L., Kållberg, P., Köhler, M., Matricardi, M., McNally, A. P., Monge-Sanz, B. M., Morcrette, J.-J., Park, B.-K., Peubey, C., de Rosnay, P., Tavolato, C., Thépaut, J.-N., and Vitart, F.: The ERA-Interim reanalysis: configuration and performance of the data assimilation system, Q. J. Roy. Meteorol. Soc., 137, 553–597, doi:10.1002/qj.828, 2011.

Feng, L. and Zhou, T.: Water vapor transport for summer precipitation over the Tibetan Plateau: multidata set analysis, J. Geophys. Res.-Atmos., 117, D20114, doi:10.1029/2011JD017012, 2012.

Gao, Y., Cuo, L., and Zhang, Y.: Changes in moisture flux over the Tibetan Plateau during 1979–2011 and possible mechanisms, J. Climate, 27, 1876–1893, doi:10.1175/JCLI-D-13-00321.1, 2014.

ESDD
5, 1159–1196, 2014

Guenther, F., Aichner, B., Siegwolf, R., Xu, B., Yao, T., and Gleixner, G.: A synthesis of hydrogen isotope variability and its hydrological significance at the Qinghai–Tibetan Plateau, Quatern. Int., 313–314, 3–16, doi:10.1016/j.quaint.2013.07.013, 2013.

Günther, F., Mügler, I., Mäusbacher, R., Daut, G., Leopold, K., Gerstmann, U. C., Xu, B., Yao, T., and Gleixner, G.: Response of dD values of sedimentary n-alkanes to variations in source water isotope signals and climate proxies at lake Nam Co, Tibetan Plateau, Quatern. Int., 236, 82–90, doi:10.1016/j.quaint.2010.12.006, 2011.

Han, Y., Fang, X., Zhao, T., Bai, H., Kang, S., and Song, L.: Suppression of precipitation by dust particles originated in the Tibetan Plateau, Atmos. Environ., 43, 568–574, doi:10.1016/j.atmosenv.2008.10.018, 2009.

Hren, M. T., Bookhagen, B., Blisniuk, P. M., Booth, A. L., and Chamberlain, C. P.: δ^{18}O and δD of streamwaters across the Himalaya and Tibetan Plateau: implications for moisture sources and paleoelevation reconstructions, Earth. Planet. Sc. Lett., 288, 20–32, doi:10.1016/j.epsl.2009.08.041, 2009.

Immerzeel, W. W., van Beek, L. P. H., and Bierkens, M. F. P.: Climate change will affect the Asian water towers, Science, 328, 1382–1385, doi:10.1126/science.1183188, 2010.

Immerzeel, W. W., Pellicciotti, F., and Bierkens, M.: Rising river flows throughout the twenty-first century in two Himalayan glacierized watersheds, Nat. Geosci., available at: http://www.nature.com/ngeo/journal/v6/n9/abs/ngeo1896.html, last access: 3 September 2013.

Joswiak, D. R., Yao, T., Wu, G., Tian, L., and Xu, B.: Ice-core evidence of westerly and monsoon moisture contributions in the central Tibetan Plateau, J. Glaciol., 59, 56–66, doi:10.3189/2013JoG12J035, 2013.

Kang, S., Qin, D., Ren, J., Zhang, Y., Kaspari, S., Mayewski, P. A., and Hou, S.: Annual Accumulation in the Mt. Nyainqentanglha ice core, southern Tibetan Plateau, China: relationships To atmospheric circulation over Asia, Arct. Antarct. Alp. Res., 39, 663–670, doi:10.1657/1523-0430(07503)[KANG]2.0.CO;2, 2007.

Kurita, N. and Yamada, H.: The role of local moisture recycling evaluated using stable isotope data from over the middle of the Tibetan Plateau during the monsoon season, J. Hydrometeorol., 9, 760–775, doi:10.1175/2007JHM945.1, 2008.

Liu, J., Kang, S., Gong, T., and Lu, A.: Growth of a high-elevation large inland lake, associated with climate change and permafrost degradation in Tibet, Hydrol. Earth Syst. Sci., 14, 481–489, doi:10.5194/hess-14-481-2010, 2010.

ESDD
5, 1159–1196, 2014

Lu, N., Qin, J., Gao, Y., Yang, K., Trenberth, K. E., Gehne, M., and Zhu, Y.: Trends and variability in atmospheric precipitable water over the Tibetan Plateau for 2000–2010, Int. J. Climatol., doi:10.1002/joc.4064, in press, 2014.

Maussion, F., Scherer, D., Finkelnburg, R., Richters, J., Yang, W., and Yao, T.: WRF simulation of a precipitation event over the Tibetan Plateau, China – an assessment using remote sensing and ground observations, Hydrol. Earth Syst. Sci., 15, 1795–1817, doi:10.5194/hess-15-1795-2011, 2011.

Maussion, F., Scherer, D., Mölg, T., Collier, E., Curio, J., and Finkelnburg, R.: Precipitation seasonality and variability over the Tibetan Plateau as resolved by the High Asia reanalysis, J. Climate, 27, 1910–1927, doi:10.1175/JCLI-D-13-00282.1, 2014.

Mölg, T., Maussion, F., and Scherer, D.: Mid-latitude westerlies as a driver of glacier variability in monsoonal High Asia, Nat. Clim. Change, 4, 68–73, doi:10.1038/nclimate2055, 2013.

Schiemann, R., Lüthi, D., and Schär, C.: Seasonality and interannual variability of the westerly jet in the Tibetan Plateau region, J. Climate, 22, 2940–2957, doi:10.1175/2008JCLI2625.1, 2009.

Shi, X., Wang, Y., and Xu, X.: Effect of mesoscale topography over the Tibetan Plateau on summer precipitation in China: a regional model study, Geophys. Res. Lett., 35, L19707, doi:10.1029/2008GL034740, 2008.

Simmonds, I., Bi, D., and Hope, P.: Atmospheric water vapor flux and its association with rainfall over China in summer, J. Climate, 12, 1353–1367, 1999.

Skamarock, W. C. and Klemp, J. B.: A time-split nonhydrostatic atmospheric model for weather research and forecasting applications, J. Comput. Phys., 227, 3465–3485, doi:10.1016/j.jcp.2007.01.037, 2008.

Sugimoto, S., Ueno, K., and Sha, W.: Transportation of water vapor into the Tibetan Plateau in the case of a passing synoptic-scale trough, J. Meteorol. Soc. Jpn., 86, 935–949, doi:10.2151/jmsj.86.935, 2008.

Tian, L., Yao, T., MacClune, K., White, J. W. C., Schilla, A., Vaughn, B., Vachon, R., and Ichiyanagi, K.: Stable isotopic variations in west China: a consideration of moisture sources, J. Geophys. Res., 112, D10112, doi:10.1029/2006JD007718, 2007.

Trenberth, K. E.: Atmospheric Moisture Recycling: role of Advection and Local Evaporation, J. Climate, 12, 1368–1381, doi:10.1175/1520-0442(1999)012<1368:AMRROA>2.0.CO;2, 1999.

ESDD
5, 1159–1196, 2014

Webster, P., Magana, V. O., Palmer, T. N., Shukla, J., Tomas, R. A., Yanai, M., and Yasunari, T.: Monsoons: processes, predictability, and the prospects for prediction, J. Geophys. Res., 103, 14451–14510, doi:10.1029/97JC02719, 1998.

Xu, X., Lu, C., Shi, X., and Gao, S.: World water tower: an atmospheric perspective, Geophys. Res. Lett., 35, L20815, doi:10.1029/2008GL035867, 2008.

Yang, K., Ye, B., Zhou, D., Wu, B., Foken, T., Qin, J., and Zhou, Z.: Response of hydrological cycle to recent climate changes in the Tibetan Plateau, Climatic Change, 109, 517–534, doi:10.1007/s10584-011-0099-4, 2011.

Yang, K., Wu, H., Qin, J., Lin, C., Tang, W., and Chen, Y.: Recent climate changes over the Tibetan Plateau and their impacts on energy and water cycle: a review, Global Planet. Change, 112, 79–91, doi:10.1016/j.gloplacha.2013.12.001, 2014.

Yao, T., Masson-Delmotte, V., Gao, J., Yu, W., Yang, X., Risi, C., Sturm, C., Werner, M., Zhao, H., He, Y., and Ren, W.: A review of climatic controls on $\delta^{18}O$ in precipitation over the Tibetan Plateau: Observations and simulations, Rev. Geophys., 51, 525–548, doi:10.1002/rog.20023, 2013.

Zhang, Y., Wang, D., Zhai, P., Gu, G., and He, J.: Spatial distributions and seasonal variations of tropospheric water vapor content over the Tibetan Plateau, J. Climate, 26, 5637–5654, doi:10.1175/JCLI-D-12-00574.1, 2013.

ESDD
5, 1159–1196, 2014

Table 1. Decadal average of the atmospheric water flux converted to a theoretical precipitation amount (mm month^{-1}) through vertical cross sections (1, 2–3, 4–5, 6, 7, 8, 9, 10–11, 12–14) for HAR10 (positive values denote transport towards the TP, negative values denote transport away from the TP). Decadal average of the precipitation (mm month^{-1}) on the inner TP and of the contribution (%) of the atmospheric water flux to the precipitation for HAR10.

CS	1	2–3	4–5	6	7	8	9	10–11	12–14	1–14			
Month	West	SW 1–2	South 1–2	Brahmaputra	East	North-East	Qaidam	NW 5–4	NW 3–1	Sum	Inner TP Precipitation	Ratio to monthly (%)	Ratio to annual (%)
01	13.7	44.1	−5.3	6.3	−36.4	−2.2	4.0	7.7	−18.9	12.9	24.0	54 %	2 %
02	17.0	50.7	−5.0	5.8	−33.7	−2.8	4.1	8.0	−22.6	21.4	35.0	61 %	4 %
03	21.3	37.9	−6.4	8.2	−40.5	−3.1	8.7	11.9	−25.6	12.3	34.5	36 %	2 %
04	19.0	35.8	−5.0	9.7	−38.8	−3.6	10.2	11.3	−24.4	14.4	42.5	34 %	3 %
05	18.3	23.0	9.7	22.8	−47.4	−6.0	9.2	11.2	−20.4	20.2	52.4	39 %	4 %
06	3.0	28.2	20.0	23.8	−45.4	−6.9	9.7	8.3	−15.5	35.2	67.7	52 %	6 %
07	16.0	37.0	26.0	17.6	−21.0	−13.1	4.5	5.7	−24.1	48.6	92.9	52 %	9 %
08	12.5	36.1	24.0	17.3	−24.5	−13.6	6.7	7.3	−24.2	41.5	88.8	47 %	8 %
09	13.2	47.1	21.8	20.4	−59.0	−12.1	2.6	5.4	−23.4	15.9	55.4	29 %	3 %
10	16.4	22.8	10.3	19.7	−60.2	−5.4	3.9	6.7	−18.5	−4.4	22.9	−19 %	−1 %
11	18.1	26.1	−6.3	5.2	−38.0	−2.6	6.2	10.1	−21.9	−3.2	12.2	−26 %	−1 %
12	16.1	39.1	−7.0	3.6	−36.7	−2.3	5.3	9.5	−21.9	5.7	16.5	34 %	1 %
Sum (mm yr^{-1})	194.4	427.9	76.7	160.3	−481.7	−73.7	75.0	103.0	−261.4	**220.5**	**544.8**		**40 %**

ESDD
5, 1159–1196, 2014

Table 2. The same as Table 1 but for HAR30.

CS	1	2–3	4–5	6	7	8	9	10–11	12–14	1–14			
Month	West	SW 1–2	South 1–2	Brahmaputra	East	North-East	Qaidam	NW 5–4	NW 3–1	Sum	Inner TP Precipitation	Ratio to monthly (%)	Ratio to annual (%)
01	14.6	46.4	−8.5	6.9	−38.6	−2.8	4.2	8.2	−21.5	8.9	25.6	35 %	2 %
02	18.0	53.7	−7.9	6.5	−36.3	−3.5	4.5	8.7	−25.6	18.1	37.5	48 %	3 %
03	23.2	39.8	−9.8	10.0	−44.2	−3.7	9.3	13.0	−29.7	7.9	37.5	21 %	1 %
04	21.1	37.9	−9.0	12.0	−42.5	−4.0	10.9	12.1	−28.6	9.9	46.1	21 %	2 %
05	20.4	23.1	8.1	25.1	−50.9	−6.4	9.9	11.7	−24.0	17.1	57.6	30 %	3 %
06	14.5	27.1	21.7	25.0	−50.7	−7.0	10.8	8.1	−17.3	32.1	72.2	45 %	6 %
07	17.5	34.6	29.7	15.2	−25.9	−13.5	5.2	4.2	−25.8	41.3	94.5	44 %	7 %
08	13.2	34.5	27.5	15.1	−29.4	−14.4	7.5	5.6	−25.6	34.1	89.5	38 %	6 %
09	14.5	46.5	24.5	20.8	−65.4	−13.1	3.1	4.9	−26.0	9.8	56.9	17 %	2 %
10	18.4	21.7	9.2	21.3	−63.7	−6.3	4.3	7.3	−21.9	−9.6	24.5	−39 %	−2 %
11	19.8	26.4	−10.3	5.4	−40.0	−3.4	6.6	10.9	−25.4	−9.9	13.2	−75 %	−2 %
12	17.2	41.2	−10.9	3.6	−38.7	−2.9	5.6	10.2	−24.8	0.5	17.6	3 %	0 %
Sum ($mm\,yr^{-1}$)	212.4	432.9	64.3	166.8	−526.2	−80.8	82.0	104.9	−296.1	**160.1**	**572.7**		**28 %**

ESDD
5, 1159–1196, 2014

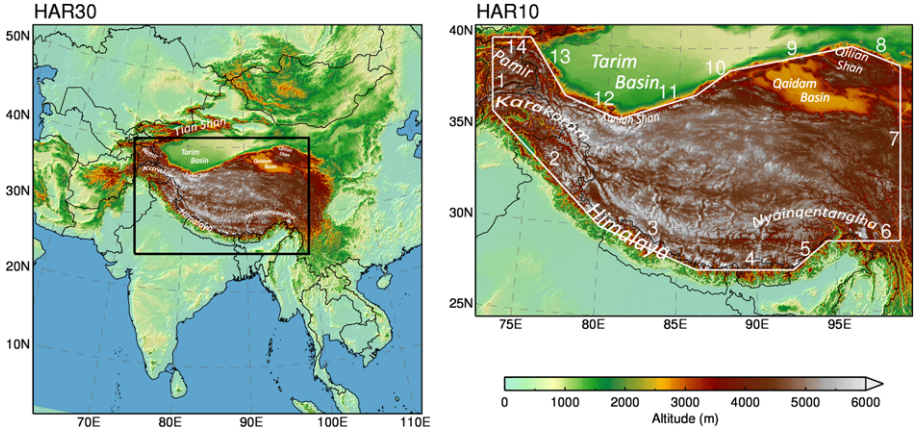

Figure 1. Maps of the WRF model domains HAR30 (south-central Asia domain, 30 km resolution) and HAR10 (High Asia domain, 10 km resolution). The transects surrounding the Tibetan Plateau (numbered 1–14) are drawn in white. The region within the defined boundaries is called "inner TP" throughout the manuscript. Geographical locations are indicated (modified after Maussion et al., 2014).

ESDD
5, 1159–1196, 2014

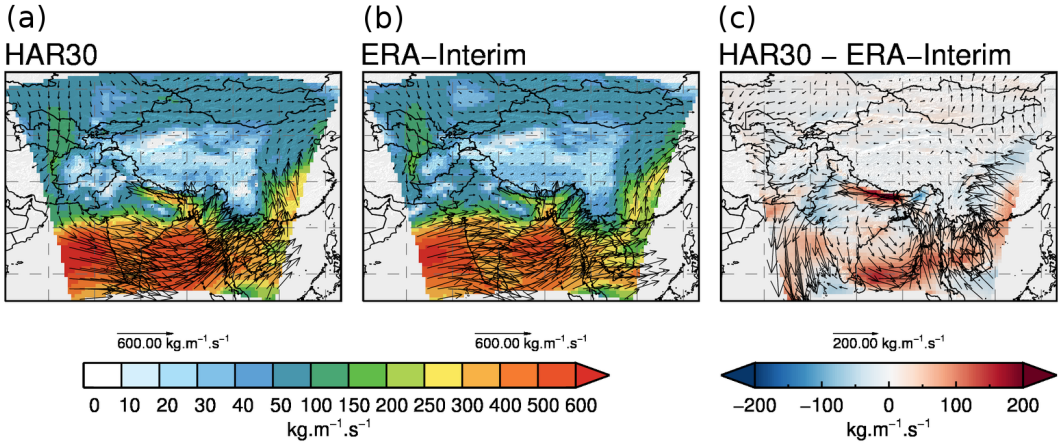

Figure 2. Decadal average of the vertically integrated water vapour flux ($kg\,m^{-1}\,s^{-1}$) in July for HAR30 **(a)**, ERA-Interim **(b)** and their difference **(c)**. The grid points without HAR30 data are masked out. Colour shading denotes strength of water vapour flux, arrows (plotted every second grid point) indicate transport direction (length of arrows proportional to flux strength up to $600\,kg\,m^{-1}\,s^{-1}$ for **(a)** and **(b)** and up to $200\,kg\,m^{-1}\,s^{-1}$ for **(c)**, constant afterwards for more readability).

ESDD
5, 1159–1196, 2014

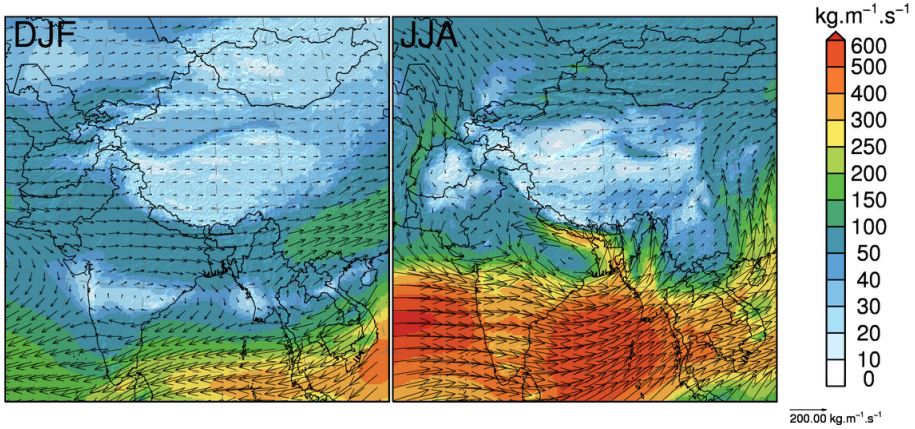

Figure 3. Decadal average of the vertically integrated water vapour flux (kg m^{-1} s^{-1}) in DJF (left panel) and JJA (right panel) for HAR30. Colour shading denotes strength of water vapour flux, arrows (plotted every sixth grid point) indicate transport direction (length of arrows proportional to flux strength up to 200 kg m^{-1} s^{-1}, constant afterwards for more readability).

ESDD
5, 1159–1196, 2014

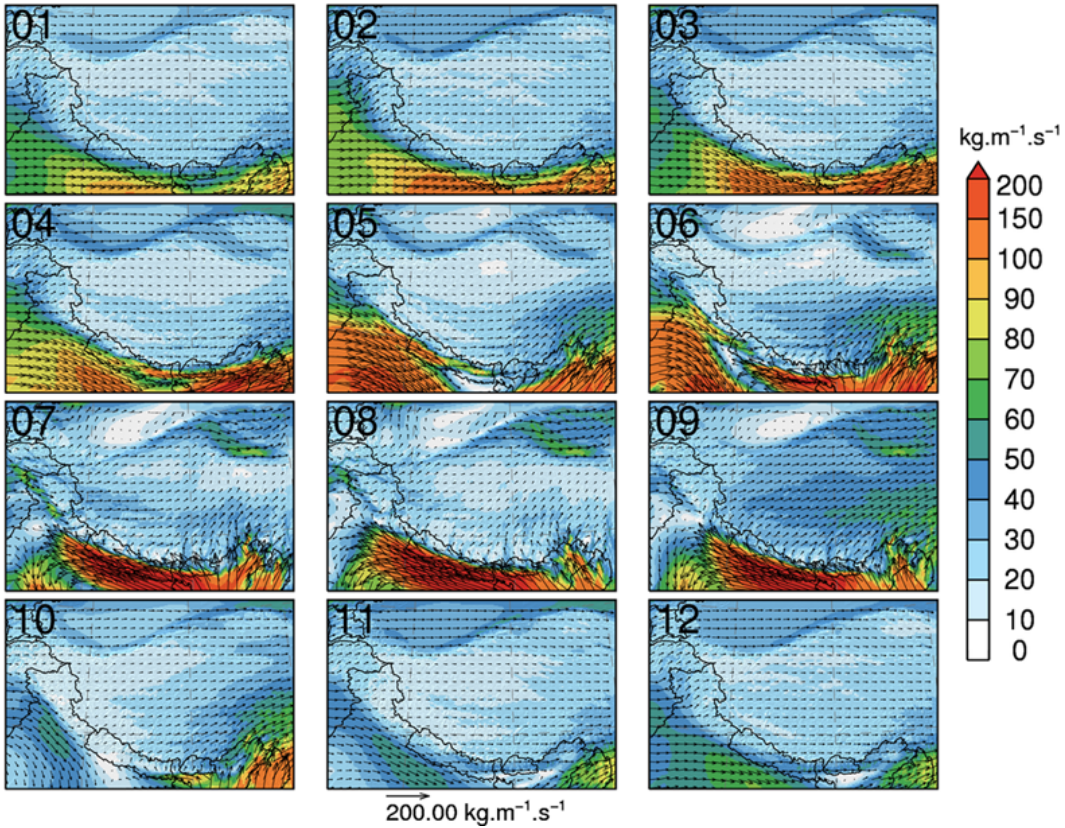

Figure 4. Decadal average of the vertically integrated water vapour flux (kg m^{-1} s^{-1}) in every month for HAR10. Colour shading denotes strength of water vapour flux, arrows (plotted every eighth grid point) indicate transport direction (length of arrows proportional to flux strength up to 200 kg m^{-1} s^{-1}, constant afterwards for more readability).

ESDD
5, 1159–1196, 2014

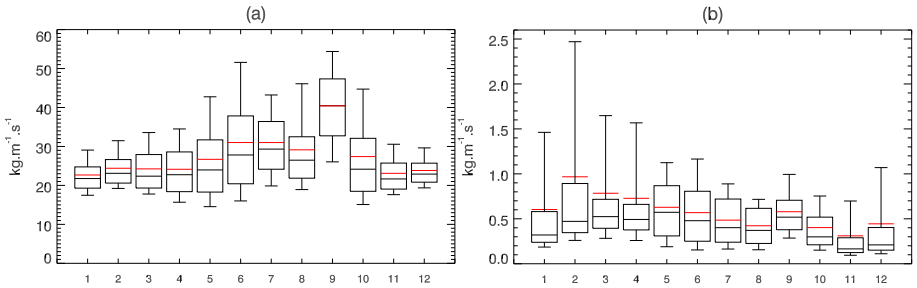

Figure 5. Box plot of the decadal average of the vertically integrated water vapour flux **(a)** and cloud particles flux **(b)** on the inner TP for HAR10 (kg m^{-1} s^{-1}). The boxes represent range from 25th percentile to the 75th percentile. The boxes are divided by the median value (black) and the mean value (red). The whiskers represent the 10th and the 90th percentile, respectively. Note the different scales of the y axes.

ESDD
5, 1159–1196, 2014

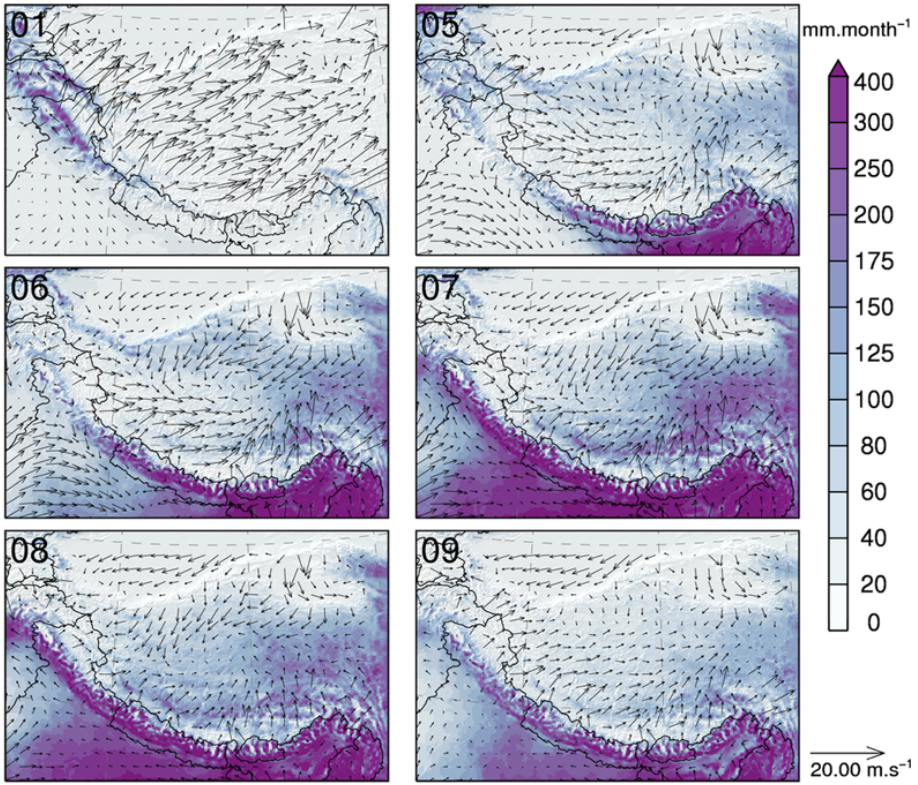

Figure 6. Decadal average of precipitation (mm month^{-1}) in January (01), May (05), June (06), July (07), August (08), and September (09) for HAR10. The arrows show the 10 m wind field (every ninth grid point plotted).

ESDD
5, 1159–1196, 2014

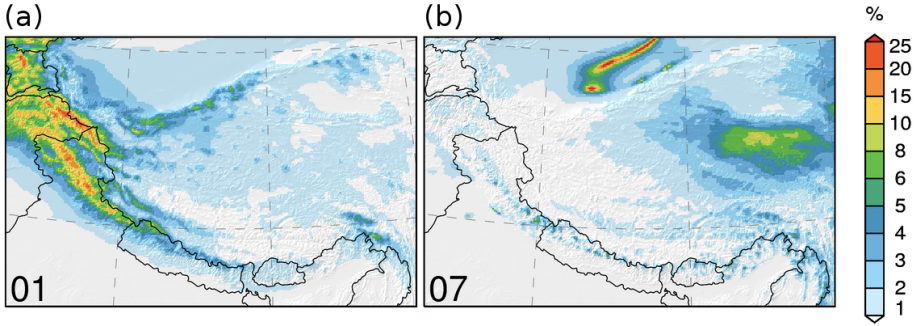

Figure 7. Decadal average of the contribution (%) of cloud particles flux to atmospheric water transport in January (01, left panel) and July (07, right panel) for HAR10.

ESDD
5, 1159–1196, 2014

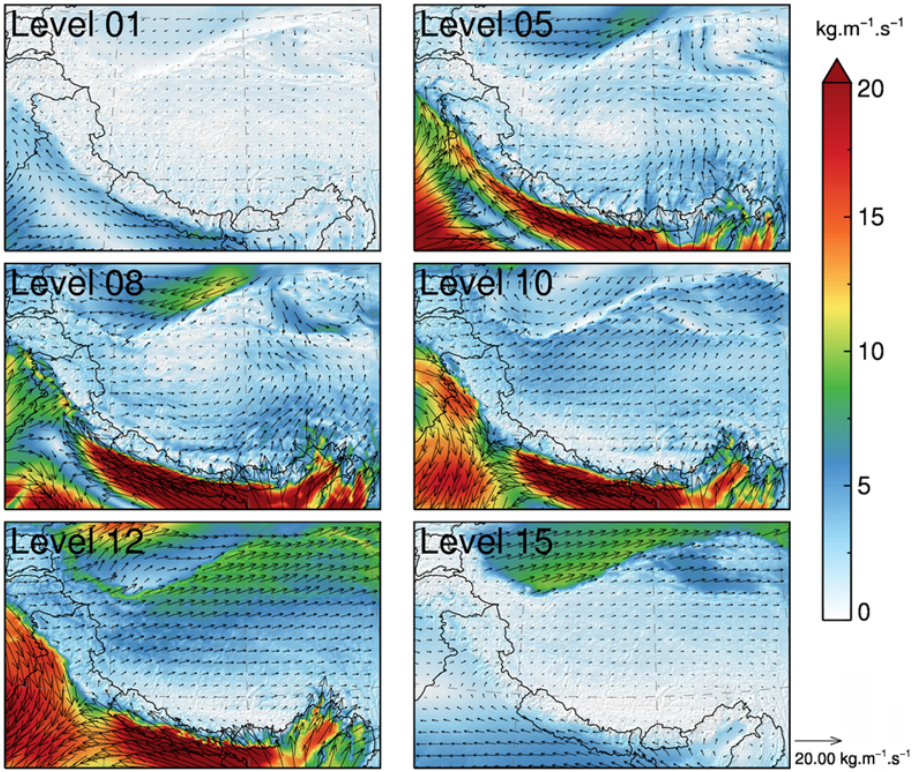

Figure 8. Decadal average of the water vapour flux ($kg\,m^{-1}\,s^{-1}$) for single selected model levels (01, 05, 08, 10, 12, 15) in July for HAR10. Colour shading denotes strength of water vapour flux, arrows (plotted every eighth grid point) indicate transport direction (length of arrows proportional to flux strength up to $20\,kg\,m^{-1}\,s^{-1}$, constant afterwards for more readability).

ESDD
5, 1159–1196, 2014

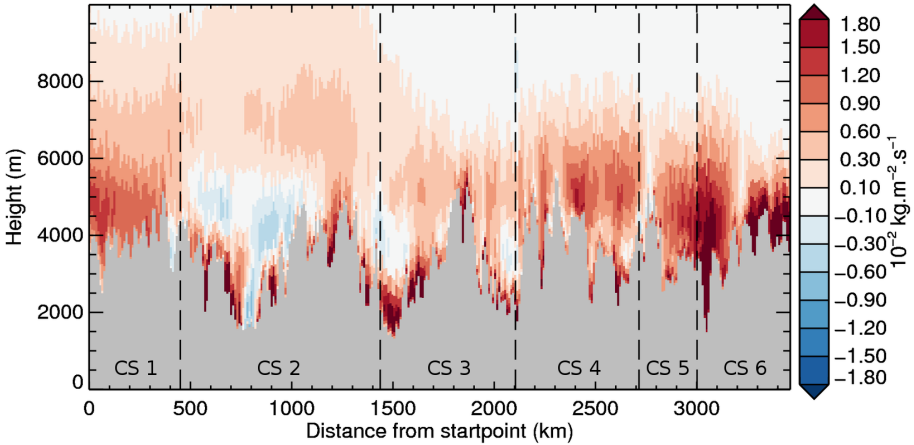

Figure 9. Decadal average of the atmospheric water transport (10^{-2} kg m^{-2} s^{-1}) for cross Sect. 1–6 (from left to right, dashed lines indicate border between the cross sections) in July for HAR10. Red colours denote transport towards the TP, while blue colours indicate transport away from the TP. The underlying topography is represented in grey.

ESDD
5, 1159–1196, 2014

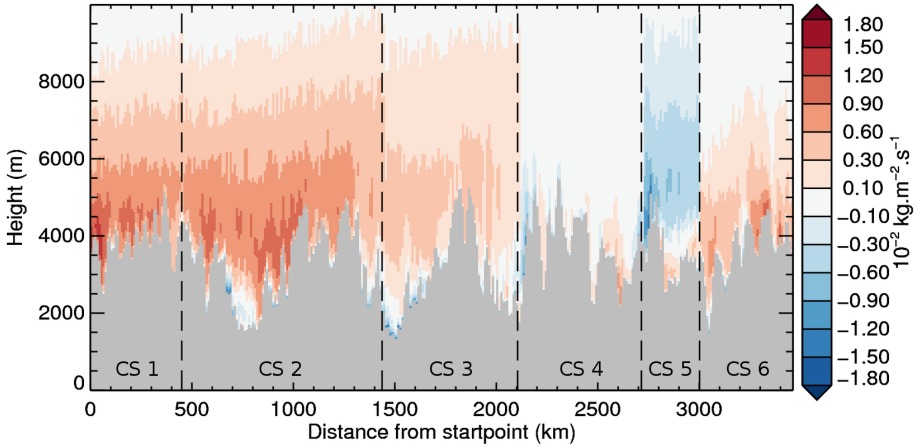

Figure 10. Same as Fig. 9 but in January.

ESDD
5, 1159–1196, 2014

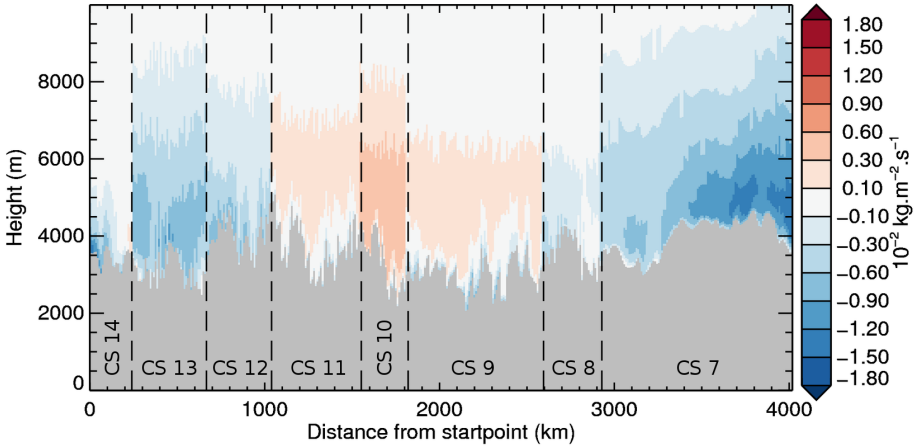

Figure 11. Decadal average of the atmospheric water transport (10^{-2} kg m^{-2} s^{-1}) for cross Sect. 14–7 (from left to right, dashed lines indicate border between the cross sections) in January for HAR10. Red colours denote transport towards the TP, while blue colours indicate transport away from the TP. The underlying topography is represented in grey.

ESDD
5, 1159–1196, 2014

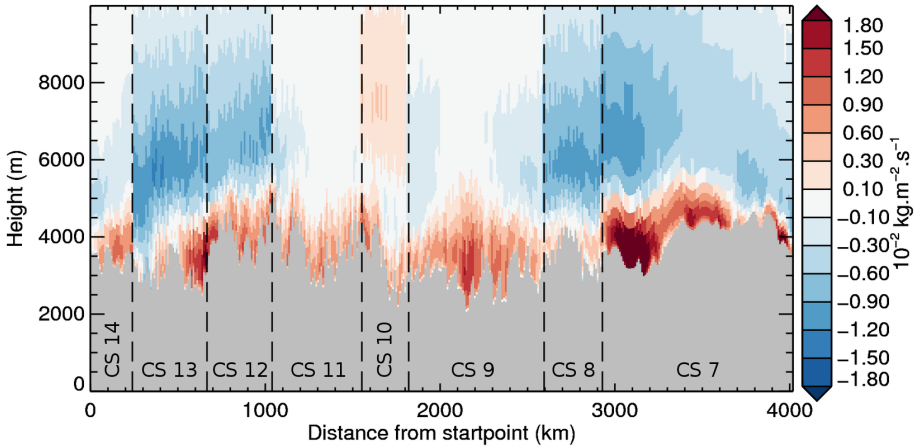

Figure 12. Same as Fig. 11 but for July.

ESDD
5, 1159–1196, 2014